Materials & Design 206 (2021) 109792

Contents lists available at ScienceDirect

Materials & Design

journal homepage: www.elsevier.com/locate/matdes

An imidazolium-based supramolecular gelator enhancing interlayer adhesion in 3D printed dual network hydrogels

Zuoxin Zhou [a], Mario Samperi [b,c], Lea Santu [a,b], Glenieliz Dizon [b], Shereen Aboarkaba [b], David Limón [d,e], Christopher Tuck [a], Lluïsa Pérez-García [c], Derek J. Irvine [a], David B. Amabilino [b], Ricky Wildman [a,*]

[a] Centre for Additive Manufacturing, Faculty of Engineering, University of Nottingham, Nottingham NG7 2RD, United Kingdom
[b] School of Chemistry and GSK Carbon Neutral Laboratories for Sustainable Chemistry, University of Nottingham, NG7 2GA, United Kingdom
[c] School of Pharmacy, University of Nottingham, NG7 2RD, United Kingdom
[d] Departament de Farmacologia, Toxicologia i Química Terapèutica, Universitat de Barcelona, 08028, Spain
[e] Institut de Nanociència i Nanotecnologia IN2UB, Universitat de Barcelona, 08028, Spain

HIGHLIGHTS

- An LMWG compound formed a supramolecular network during extrusion-based 3D printing providing structural support to the monomer.
- The monomer in all printed layers is cured simultaneously during post-processing.
- Excellent inter- and intra-layered isotropy was achieved in double-network hydrogels.
- The tensile properties were close to those fabricated using mould casting.
- The gelator fibrillar network was embedded and physically interpenetrated in the polymer structure.

GRAPHICAL ABSTRACT

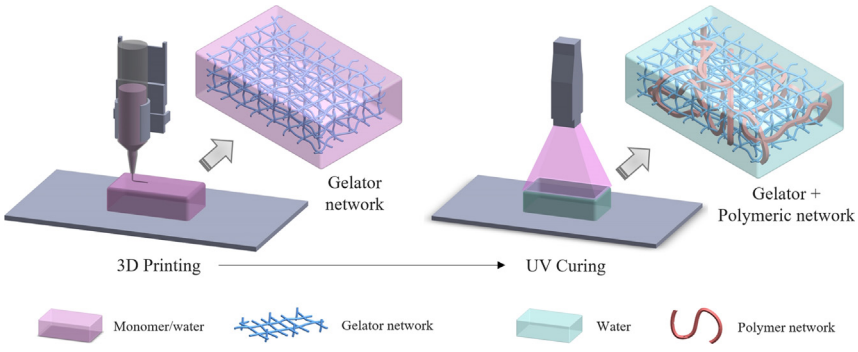

ARTICLE INFO

Article history:
Received 15 January 2021
Revised 12 April 2021
Accepted 2 May 2021
Available online 5 May 2021

Keywords:
3D printing
Additive manufacturing
Low molecular weight gelator
Supramolecular
UV-curable monomer
Double-network hydrogel

ABSTRACT

The variety of UV-curable monomers for 3D printing is limited by a requirement for rapid curing after each sweep depositing a layer. This study proposes to trigger supramolecular self-assembly during the process by a gemini imidazolium-based low-molecular-weight gelator, allowing printing of certain monomers. The as-printed hydrogel structures were supported by a gelator network immobilising monomer:water solutions. A thixotropic hydrogel was formed with a recovery time of <50 s, storage modulus = 8.1 kPa and yield stress = 18 Pa, processable using material extrusion 3D printing. Material extrusion 3D printed objects are usually highly anisotropic, but in this case the gelator network improved the isotropy by subverting the usual layer-by-layer curing strategy. The monomer in all printed layers was cured simultaneously during post-processing to form a continuous polymeric network. The two networks then physically interpenetrate to enhance mechanical performance. The double network hydrogels fabricated with layers cured simultaneously showed 62–147% increases in tensile properties compared to layer-by-layer cured hydrogels. The results demonstrated excellent inter- and intra-layered coalescence.

* Corresponding author.
E-mail address: ricky.wildman@nottingham.ac.uk (R. Wildman).

https://doi.org/10.1016/j.matdes.2021.109792

Consequently, the tensile properties of 3D printed hydrogels were close to mould cast objects. This study has demonstrated the benefits of using gelators to expand the variety of 3D printable monomers and shown improved isotropy to offer excellent mechanical performances.

1. Introduction

Photopolymerisation pathways are established in 3D printing processes such as vat polymerisation, materials jetting and material extrusion [1–5]. The monomers/oligomers used in 3D photopolymerisation contain photosensitive functional groups including methacrylates, acrylates and acrylamides, which can polymerise under ultraviolet (UV) radiation. The advantage of photopolymerisation in 3D printing is the fast cure time which provides a rapid and stable phase change into the solid. It allows liquid materials to be dispensed in a variety of ways and achieve high resolution from a localised light source [6,7]. Photopolymerisation has also been widely used to provide a covalent network for hydrogels in 3D printing [8,9]. However, 3D photopolymerisation has a key limitation: the processed materials must reach a high degree of cure in a very short processing period [10–13]. This factor is particularly crucial for 3D printing of hydrogels with high water content (ca. >80%), as a rigid covalent network needs to form rapidly upon deposition. The curing kinetics of photopolymerisation depend strongly on the type and number of photosensitive functional groups, the size of pendant groups, and the presence of oxygen [14–16]. Consequently, most of the 3D printing photocurable resins comprise multifunctional monomers such as diacrylate and tri-acrylate in order to favour rapid curing rates during the process [17–19]. Unfortunately, many potentially useful photocurable monomers/oligomers are excluded from 3D printing manufacturing because of their slow curing rates. However, this problem could be circumvented if a secondary network could be established to support the hydrogel structure during 3D printing, then allowing the photocurable monomers to cure over longer timescales.

In the specific case of material extrusion 3D printing, another challenge in the preparation of robust printed objects is to achieve good interlayer adhesion. Mechanical anisotropy for extrusion printed objects is a significant problem because molecular chain entanglement in the interlayered regions is limited [20–23]. Consequently, molecular chain entanglement and orientation in cast objects are usually more isotropic than those prepared using material extrusion 3D printing [24,25]. In many printed materials, the bonding between layers of material is weak, leading to stress concentration and premature failure. While some elegant approaches to interlayer adhesion have been devised there is still a need for a simple, general method to achieve good interlayer adhesion [21,26–29]

To overcome the abovementioned problems, low-molecular-weight gelators (LMWG) are proposed to act as a fast-forming network to support a hydrogel that is more made robust via a photopolymerisation to give a covalent network [30,31]. The self-assembly of LMWGs can be triggered by various mechanisms (such as temperature, pH and solvent polarity changes, and ultrasound) generating relatively soft networks through supramolecular interactions (e.g. hydrogen-bonding, π-stacking, and van der Waals interactions) that entrap and immobilise solvents with a much larger volume as a result of high surface tension [30–32]. Previously, supramolecular chemistry has been used to modify natural or create synthetic polymers for 3D printing purposes [22,29]. For example, a recent study has used thermo-reversible gelatin to provide structural support for 3D bioinks [29]. Supramolecular gels can form networks with very small loading of the LWMGs (e.g. 0.5 ~ 3 wt%) because of the nature of the small molecules and therefore the bulk properties of the functional materials are retained. Attempts to develop 3D printable LMWGs have only recently emerged, including the creation of a gelator network which can support 3D printed structures containing dimethylsulfoxide (DMSO) [33,34]. Solvents can be removed after gel formation potentially making the porous materials useful for tissue engineering. However, it would be of greater interest to investigate more functionalised 3D printing formulations consisting of gelator and functional monomers. This combination of structural components can potentially form softer non-covalent networks and harder covalent networks in the same material. This concept of double-network (DN) gels has attracted considerable attention in the material science field [35–38]. The principal polymeric network mainly contributes to the rigidity of the hydrogel but in general is also brittle. The secondary gelator network provides toughness, fatigue resistance and self-healing to the polymeric network owing to the uniquely self-recovery properties that can be triggered spontaneously in the non-covalent interactions [38–40]. DN gels have been used to improve the mechanical strength and toughness of hydrogel with high water content (*ca.* 90%) [41]. It is a particularly interesting approach for certain tissue engineering applications that require highly robust and biocompatible implants.

Motivated by our previous work on LMWGs [42], we incorporated the imidazolium-based amphiphile **1·2Cl** (Fig. 1) in 3D printing formulations to form DN networks with covalent and non-covalent interactions. The selection of the cationic gemini amphiphile to form supramolecular gels is that they confer unique properties in regard to exchanging the counter-ion and the gelator can be made on the multigram scale with relative ease. Indeed, our previous work shows that this class of amphiphiles are (a) synthetically accessible, (b) non-toxic, (c) capable of self-assembly in supramolecular architectures forming soft materials, (d) recognize and transport biologically relevant compounds such anions (carboxylates, chlorides, phosphates) and neurotransmitters (dopamine, serotonin), (e) can stabilise gold and silicon surfaces, and (f) can encapsulate and release a variety of structurally diverse drugs in biological media [43]. These type of gels are extremely easy and fast to prepare (in mixtures of ethanol and water) and highly versatile in the amount and type of drug that can be incorporated into their fibres [44,45]. This gelator is first dissolved in solvents such as ethanol [42,46]. It starts to self-assemble via hydrophobic association after mixing with water, which serves as an anti-solvent. The hydrophobic chains in the gelator interdigitate as the charged hydrophilic segments remain exposed to the solvent [44]. The tightly associated molecules increase the toughness of the hydrogels where the fibres are physically crosslinked. Hydrophobic association have attracted attention because of their ability to spontaneously reassociate supramolecular interaction after damage [47–49]. The hydrophobic chains can be rearranged back to the hydrophobic domains after any external forces are removed from the hydrogel [47,50]. The ability to reassociate the amphiphilic molecules back to their initial state leads to thixotropic properties. In general, thixotropic hydrogels are ideal for extrusion-based 3D printing technique if it recovers over a short period of time [46,51,52]. The thixotropy allows the reformation

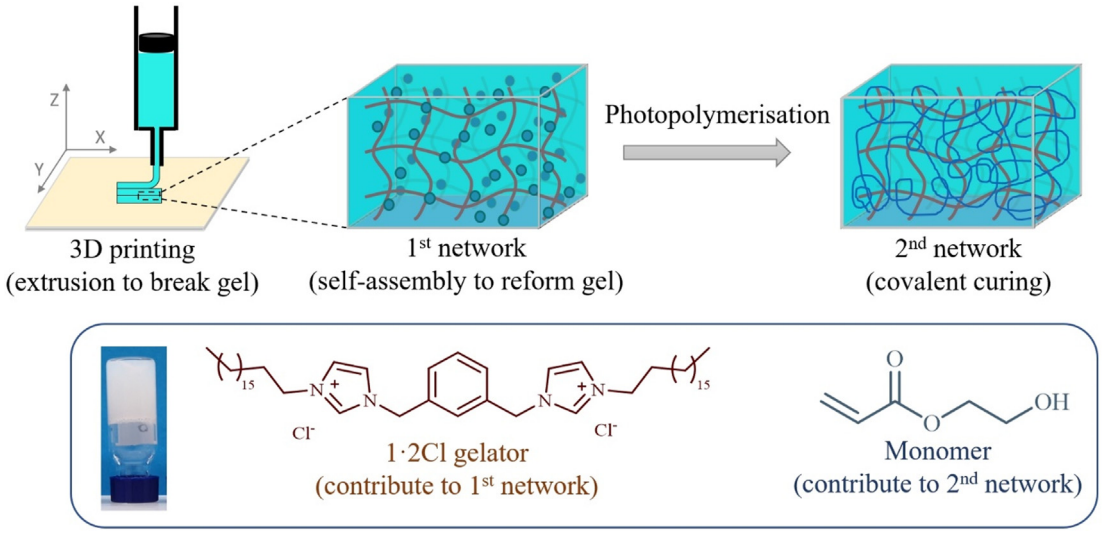

Fig. 1. The formation process of DN hydrogel through supramolecular interaction and covalent curing. An extrusion-based 3D printing broke the gel form which was re-formed via gelator self-assembly to establish the 1st network. The 2nd polymeric network was formed by photopolymerisation. The chemical structure of **1·2Cl** gelator and hydroxyethyl acrylate (as an example of the monomer candidate) were shown which contributed to the formation of the 1st and 2nd networks, respectively.

of an elastic hydrogel upon deposition to support multi-layer stacking of a 3D printed structure [52]. Other desirable rheological properties for a 3D printable hydrogel also include shear thinning behaviour allowing the hydrogel to flow easily and sufficient stiffness and yield stress for material retention prior to crosslinking [53]. The potential capability of forming tough and thixotropic hydrogels led us to use **1·2Cl** as the gelator material to investigate in this study. On a longer timescale, these properties are potentially capable of maintaining the structural integrity of the 3D printed hydrogel until the monomer is fully cured to achieve the desirable mechanical properties of the final product.

The aim of this research was to develop a DN hydrogel formulation that used a supramolecular gelator network to provide structural support during an extrusion-based 3D printing process. The capability of the gelator to form hydrogels with different monomers, the processing and post-processing curing parameters, and characterisation of the 3D printed DN hydrogels – in particular their mechanical properties – were investigated.

2. Materials and methods

The hypothesis of this study was that an LMWG compound **1·2Cl** forms a supramolecular network during extrusion-based 3D printing which provides sufficient structural support to the monomer, and a DN hydrogel is therefore fabricated via photopolymerisation of the monomer during postprocessing. To test this hypothesis, a four-step experimental programme was conducted including (1) identification of monomer candidates to form hydrogels with **1·2Cl** via screening; (2) determination of extrusion printability by rheological assessment; (3) optimisation of 3D printing and post-processing curing parameter; (4) evaluation of the effects of supramolecular network on the isotropy of 3D printed structures. The methods of each step are explained in detail in this section.

2.1. Materials

The LMWG compound **1·2Cl** was prepared using a route adapted from the analogous bromide salt [42,46], details in **Supplementary**. Eleven UV-curable monomers were purchased from Sigma-Aldrich and investigated in this study: *N*-[3-(Dimethylamino)propyl]acrylamide (DMLPam), 2-hydroxyethyl acrylate (HEA), 2-hydroxyethyl methacrylate (HEMA), 2-carboxyethyl acrylate (CEA), hydroxypropyl acrylate (HPA), 3-chloro-2-hydroxypropyl methacrylate (ClHPMA), ethyl methacrylate (EMA), benzyl methacrylate (BMA), isobornyl methacrylate (iBnMA), hexyl methacrylate (HMA), and lauryl methacrylate (LMA). Irgacure 2959 was used as the photoinitiator (PI) in this study. It is the only FDA-certified PI that can be safely used in aqueous photocuring systems such as hydrogels and bioinks. Irgacure 2959 (Ciba-Geigy AG, Switzerland) is most efficiently activated under 365 nm UV wavelength.

2.2. Hydrogel formulation development

Each of the eleven monomer candidates were mixed with **1·2Cl** and then combined with water to assess (1) if the gelator powder was soluble in the monomer and (2) if the monomer is miscible with water. The gelator was mixed with monomer:water solvents to give a final concentration of 5 mg/ml. The volumetric percentage of monomers varied between 10% and 40%. After identifying the candidate monomers, the capability of gelation was assessed for each of them. **1·2Cl** was first dissolved in the monomer followed by addition of water at room temperature. A successful gel formation was determined by inverting the sample tube initially, by which promising gel formation was taken here as when no liquid was released from the material after inverting the sample vial for 1 min.

Using the aforementioned approach, several monomer:water combinations were identified as candidates for gelation by **1·2Cl**. Hydrogels are hydrophilic 3D networks that contain a large amount of water especially important for biomedical applications. The resulting polymers from DMLPAm, HEA, and HEMA have sufficiently high-water solubility and hydrophilicity for them to form polymeric hydrogels. Hydrogels containing each of these three polymers are widely investigated towards tissue engineering applications, such as carriers for delivery of bioactive molecules and 3D structures acting as support for tissue formation [54–61]. An initial assessment of potential monomer candidates revealed that HEA has the fastest gelation with **1·2Cl** in water, suggesting suitability for 3D printing. After curing, the poly(2-hydroxyethyl acrylate) (PHEA) formed is a biocompatible material with low cyto-

toxicity, good cell compatibility and thermal stability [62–65]. These properties, and those of the equivalent methacrylate, make both hydrogels suitable for use in drug delivery systems, implants, and contact lenses [62,66] The PHEA hydrogel is the more hydrophilic of the two, leading to a potentially greater water absorption and cell attachment if implanted *in vivo*. For these reasons, this study specifically focussed on HEA for further investigation of 3D printability of hydrogel formulations. The hydrogel formulations containing **1·2Cl** and HEA were henceforth referred to as **1·2Cl-HEA**. The polymeric hydrogel after curing is abbreviated **1·2Cl-PHEA**. Different formulations were prepared by mixing HEA, water and gelator at different water:monomer ratio (6:4, 7:3, 8:2, and 9:1) and gelator concentration (5, 7.5, and 10 mg/ml), all in 1 ml total solution volume. The photoinitiator (PI) was further added to the formulations at 1.5 mg/ml. For formulations containing PI, additional concentrations of gelator were considered (20 and 30 mg/ml) since there were likely to be negative effects on the gelation resulting from PI addition. Immediately after mixing, each solution was transferred to a 1 ml syringe where the gelation occurred. Each of the gels was then injected into a 1 ml glass vial. By pressing the syringe plunger by hand, the elastic gel was broken into a viscous liquid. The time required to reform a self-supportive gel (t_{re}) was recorded using the same inverting method. Gels demonstrating rapid fibre reassembly, ideally < 1 min, were considered as promising formulations to be used in extrusion-based 3D printing.

2.3. Rheology of the hydrogel formulation

Oscillatory rheology was carried out using a Kinexus Pro rheometer (Malvern Instruments, United Kingdom). Measurements were performed in an oscillatory shear mode using a parallel plate geometer with 0.2 mm gap at 25 °C. The selected **1·2Cl-HEA** hydrogel formulation was tested under (1) amplitude sweeps, (2) frequency sweeps, and (3) cyclic high shear rate-low shear strain rheological process. The linear viscoelastic region was determined using the amplitude sweeping mode at 1 Hz. The test sample was exposed to shear stresses up to beyond the yield stress. The yield stress was determined at the crossover point of storage modulus/loss modulus (G′/G″) [53]. Frequency sweeps from 0.4 to 10 Hz were carried out at a constant shear stress of 5 Pa predetermined from the linear viscoelastic limit of the hydrogel under test. The thixotropic properties of the hydrogel were investigated using the cyclic high shear rate-low shear strain rheological process. Initially the tested hydrogel was maintained at low shear strain of 0.01% for 120 s. After the initial stage, it was subjected to high shear rate at 10 s^{-1} for 30 s to destroy the gel. Subsequently the test was returned to a lower shear strain of 0.01% for 300 s to allow recovery. A total of eight cycles were performed.

2.4. 3D printing of the hydrogel formulation

The direct dispensing head of a 3D Discovery™ Evolution 3D bioprinter (regenHU, USA) was used in this study to print the hydrogel. It uses a high-precision plunger dispenser to extrude the hydrogel out from a nozzle and deposit it onto a substrate to construct 3D objects. Immediately after mixing, the **1·2Cl-HEA** formulation in liquid form was transferred to a 3 ml polypropylene syringe. It was kept vertically on the bench for 4 h at the lab temperature (controlled at approx. 22 °C) to allow the gel network to form. Subsequently the syringe was installed inside the 3D printer and connected with a needle of 0.6 mm diameter. Firstly, various printing speeds (i.e. printhead movement speed), from 5 mm/s to 15 mm/sec, were tested to deposit the hydrogel. A constant pressure of 15 Pa was set up for all printing speeds. Four parallel filaments of 25 mm length were printed on glass slides. For each printed filament five width measurements were taken at different positions. The consistency in printing quality was then compared to determine the optimum printing speed. The height of printed filament that was also measured to determine the setup of layer thickness.

Following processing parameter optimisation, the post-processing UV curing on 3D printed hydrogels was also investigated. The hydrogel was 3D printed to form a five-layer structure with layer thickness of 0.8 mm (Fig. 2). During post-processing, the printed hydrogels were exposed to 365 nm UV wavelength using a FireFly UV LED curing system (FJ100, Phoseon Technology, USA). UV curing was carried out in a closed environment so that a high humidity level (>90%) generated using a humidifier can be maintained. A high humidity level significantly reduced water evaporation from the hydrogel under prolonged UV curing. Effects of curing time on the conversion of HEA under air and nitrogen (N_2) atmosphere were investigated. Under N_2, the UV curing setup was placed inside a sealed glove box in which the oxygen level was maintained below 1%. The printed hydrogels were cured for 0, 5, 10, 20, 30, and 60 min. Each hydrogel after curing was analysed using a Tensor Fourier-transform infrared spectroscopy (FTIR) (Bruker, USA). The reduction in vinyl group was determined by calculating the ratios of peak intensities associated with C=C and C=O bonds in the material. The two distinctive peaks were observed at 1730 cm^{-1} and 1650 cm^{-1} representing C=O and C=C stretching. The C=O bonds remained unaffected during polymerisation while C=C bonds were reduced in the reactions. The reduction in vinyl group Δ (%) is calculated using the following equation[5]:

$$\Delta = \left(1 - \frac{I_{C=C}/I_{C=O}}{I'_{C=C}/I'_{C=O}}\right) \times 100\%$$

where $I_{C=C}$, $I_{C=O}$, $I'_{C=C}$ and $I'_{C=O}$ are the peak intensities in the FTIR spectra related to the C=C and C=O groups in the polymerised structures and non-polymerised structures (curing time = 0 min).

Following the optimisation of the processing and post-processing, different 3D structures were printed with the **1·2Cl-HEA** hydrogel formulation including a multi-layered flower-shaped structure to demonstrate 3D printing capability.

2.5. Characterisation of the DN hydrogels

Tensile testing dumbbell samples were designed according to ISO 527-1:1996 with a gauge length of 10 mm and sample thickness of 2.4 mm. Three groups of 3D printed hydrogels and two groups of mould cast hydrogels were investigated in terms of their tensile properties. The mould casting method used a tensile-sample mould that can fabricate the identical dumbbell structure as the planned 3D printed structure. The details of each tested groups of hydrogels are as follows:

3D printing group 1: For each layer, the filament was deposited in a vertical pattern that was perpendicular to the tensile forces later applied to the hydrogels during testing. All layers were cured simultaneously during post-processing.

3D printing group 2: For each layer, the filament was deposited in a horizontal pattern that was parallel to the tensile forces later applied to the hydrogels during testing. All layers were cured together during post-processing.

3D printing group 3: For each layer, the filament was deposited in a vertical pattern that was perpendicular to the tensile forces later applied to the hydrogels during testing. Each layer was cured after being printed using the same curing condition. The subsequent layer was then printed onto the cured layer, therefore layer-by-layer curing was achieved for this group of samples.

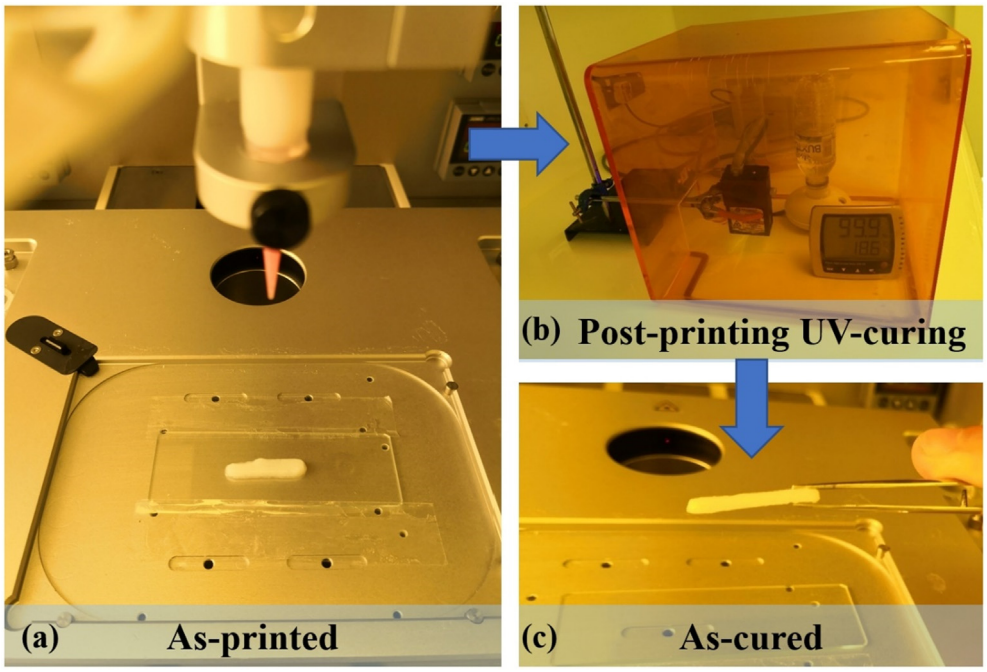

Fig. 2. (**a**) 3D printing process and (**b**) postprocessing setup of UV-curing in this study. An example of the (**a**) as-printed **1·2Cl-HEA** and (**c**) as-cured **1·2Cl-PHEA** hydrogels are shown.

Mould casting group 1: the **1·2Cl-HEA** hydrogels were cast into the mould and cured into **1·2Cl-PHEA** samples with the same curing conditions as the 3D printing groups.

Mould casting group 2: the HEA:water solution (i.e. no gelator) was cast into the mould and cured into PHEA samples with the same curing conditions as the 3D printing groups.

Tensile testing was carried out using an Instron 5966 tensile tester (Instron, USA) with a 5 kN load cell. A minimum of four tensile samples for each group was loaded to failure at crosshead speeds of 5 $mm.min^{-1}$. The dimensions of each tested sample were measured using a micro-meter prior to the testing. Young's modulus, tensile stress to break and elongation were determined from the stress vs. strain data. The statistical significance between tested groups was calculated using one-way Analysis of Variance (ANOVA) with post-hoc Bonferroni correction based on normal probability tests. A p-value less than 0.05 was used to denote significance.

The sample morphology of **1·2Cl-PHEA** and PHEA were imaged using a JEOL 7100F Field Emission Gun Scanning Electron Microscopy (SEM) (Zeiss, Germany). The imaged structures were mounted on an aluminium stub. They were dried under vacuum at room temperature for 2 days to evaporate solvent following by iridium coating to give a 5-nm thick layer. The SEM was operated at 5 kV accelerating voltage and a working distance of 10 mm.

X-ray diffraction (XRD) and FTIR analysis was conducted on the **1·2Cl-PHEA**, PHEA, and **1·2Cl**. A Bruker D8 Advance Series 2 XRD and a Bruker Tensor FTIR (Bruker, USA) were used to identify the phases present in the different sample types.

3. Results and discussion

3.1. Formulating Imidazolium-based LMWG hydrogels for 3D printing

A systematic screening of acrylate/methacrylate monomers for gelability with **1·2Cl** and water was carried out. First, six of the eleven monomers (Fig. 3) were found to dissolve the **1·2Cl** gelator at 5 mg/ml. Among them, three monomers (DMLPAm, HEA and HEMA) were capable of forming hydrogels after adding water as an anti-solvent to trigger hydrophobic gelator association. We observed that there was a strong correlation between gelation and the partition coefficient (log P) of the monomers (Fig. 3). In this study, the thereotical values of log P (a parameter that represents the polarity of each monomer is) were calculated from MarvinSketch software (version 17.26, ChemAxon) after introducing the chemical structures. Monomers that achieved **1·2Cl** solubility had log $P \leq 1.34$; they achieved gelation with log $P \leq 0.62$. As demonstrated, a monomer with low log P can trigger hydrophobic association gelation from **1·2Cl** self-assembly. Low log P allowed the monomers to have water miscibility and forced the amphiphilic **1·2Cl** to aggregate into fibres. Our previous study has shown that the hydrophobic segments in the molecule self-assemble as the surrounding solution was highly hydrophilic (Fig. 2) [44]. This mechanism successfully led to the formation of supramolecular hydrogels.

For extrusion-based 3D printing, it is crucial that the gelator fibres can be rapidly reassembled after the gel is broken by extruding out of a small nozzle. The reassembly speed of **1·2Cl** was affected by the concentrations of each component in the formulation: water, monomer, gelator, and PI. After conducting a sweep of water:HEA and gelator concentration to understand the reassembly time, we were able to identify that a water:HEA ratio of 80:20 resulted in significantly shorter reassembly times than at other ratios (Fig. 4). This was observed to be true for a range of gelator concentrations. Increasing the water content to 90% retained some of reassembly properties, but at a significantly slower rate than at 80%. Reducing the water to below 80% resulted in a very marked increase in reassembly time. Additionally, the impact of PI was significant on the t_{re}. To achieve $t_{re} < 30$ s, a 30 mg/ml **1·2Cl** concentration was required after 1.5 mg/ml PI was added in the formulation. The PI apparently inhibits fibre growth of the gelator. Therefore, higher gelator concentration was required to compensate the negative impact of PI on the t_{re}.

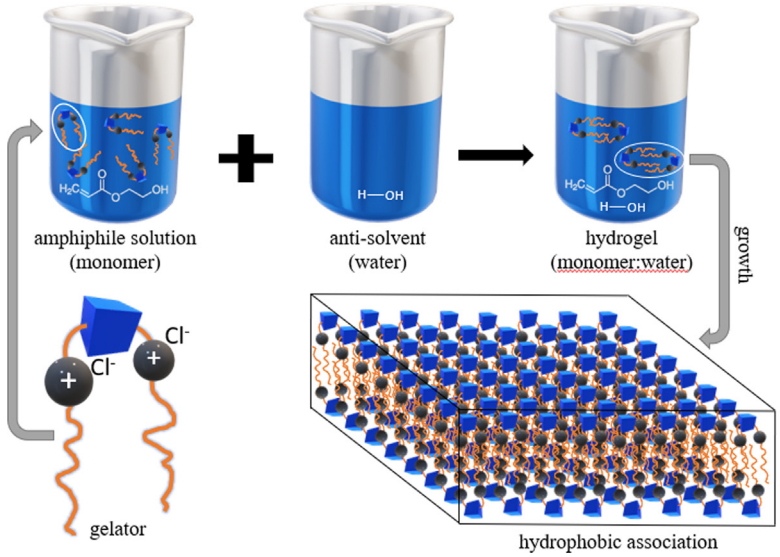

Monomer	logP	Gelator Solubility	Water Miscibility	Form
DMLPAm	0.03	Soluble	Miscible	Gel
HEA	0.22	Soluble	Miscible	Gel
HEMA	0.62	Soluble	Miscible	Gel
CEA	0.63	Soluble	Immiscible	
HPA	0.64	Soluble	Miscible	Sol
CHPMA	1.34	Soluble	Immiscible	
EMA	1.66	Insoluble	Immiscible	
BMA	2.9	Insoluble	Immiscible	
IBNMA	3.82	Insoluble	Immiscible	
HMA	4	Insoluble	Immiscible	
LMA	6.19	Insoluble	Immiscible	

Fig. 3. The monomer candidates that demonstrated gel formation capability with the **1·2Cl** gelator at 5 mg/ml. Monomers were sorted in the table by logP from lowest to highest (**right**). Positive results are highlighted in blue. Gel: gel formation. Sol: solution. A schematic of the gel formation on a molecular level is presented (**left**). DMLPam: *N*-[3-(Dimethylamino)propyl]acrylamide, HEA: 2-hydroxyethyl acrylate, HEMA: 2-hydroxyethyl methacrylate, CEA: 2-carboxyethyl acrylate, HPA: hydroxypropyl acrylate, ClHPMA: 3-chloro-2-hydroxypropyl methacrylate, EMA: ethyl methacrylate, BMA: benzyl methacrylate, iBnMA: isobornyl methacrylate, HMA: hexyl methacrylate, LMA: lauryl methacrylate. (For interpretation of the references to colour in this figure legend, the reader is referred to the web version of this article.)

Monomer	Water (vol.%)	Gelator (mg/ml)	PI (mg/ml)	t_{re}
HEA	60	5	0	>8 min
	60	7.5	0	>8 min
	60	10	0	>8 min
	70	5	0	>8 min
	70	7.5	0	>8min
	70	10	0	>8 min
	80	5	0	>8 min
	80	7.5	0	4-8 min
	80	10	0	<30 sec
	90	10	0	4-8 min
HEA	80	10	1.5	> 8min
	80	20	1.5	> 8 min
	80	30	1.5	<30 sec
	90	10	1.5	> 8 min

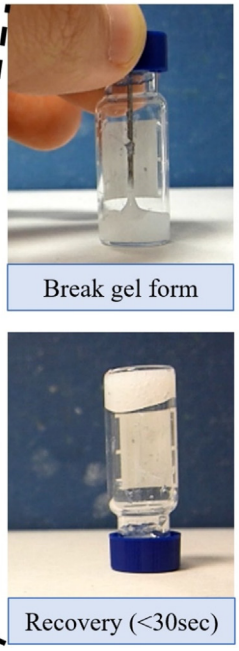

Fig. 4. The gel re-assembly time (t_{re}) of different HEA hydrogel formulations by varying water, gelator, and PI concentrations. The most promising results for application in 3D printing are highlighted in blue. The photographs show a broken (top) and recovered (bottom) gel formed by **1.2Cl** in HEA:water with PI present. (For interpretation of the references to colour in this figure legend, the reader is referred to the web version of this article.)

It is important to characterise the rheological behaviour of a 3D printed hydrogel formulation. The stiffness, thixotropy, recovery time, and yield stress all have significant impact in determining the success of an extrusion-based 3D printing process. After applying high shear rate at 10 s^{-1}, the G′ decreased greatly from approximate 8000 Pa to below 0.5 Pa (Fig. 5(**a**)). The G″ also exceeded G′ under high shearing, indicating the hydrogel was transferred from a more solid-like state (elastic) to a more liquid-like state (viscous). The fibrous network formed by the non-covalently bonded **1·2Cl** molecules is disassociated under high shearing and the previously entrapped solvent allowed to flow. Therefore, the gel was essentially converted into a liquid. However, the loss of stiffness was rapidly recovered after high shear was removed from the hydrogel. On average, after 57 s the G′ had recovered to 85% of the original value prior to the high shear rate. This period is generally regarded as the recovery time for a thixotropic material. Additionally, G′ was higher than G″ under low shear because of the self-assembled fibrillar network entrapping solvent between the strands again. For a typical extrusion-based 3D printing process, materials are subjected initially to relatively low shear rate, following by high shear

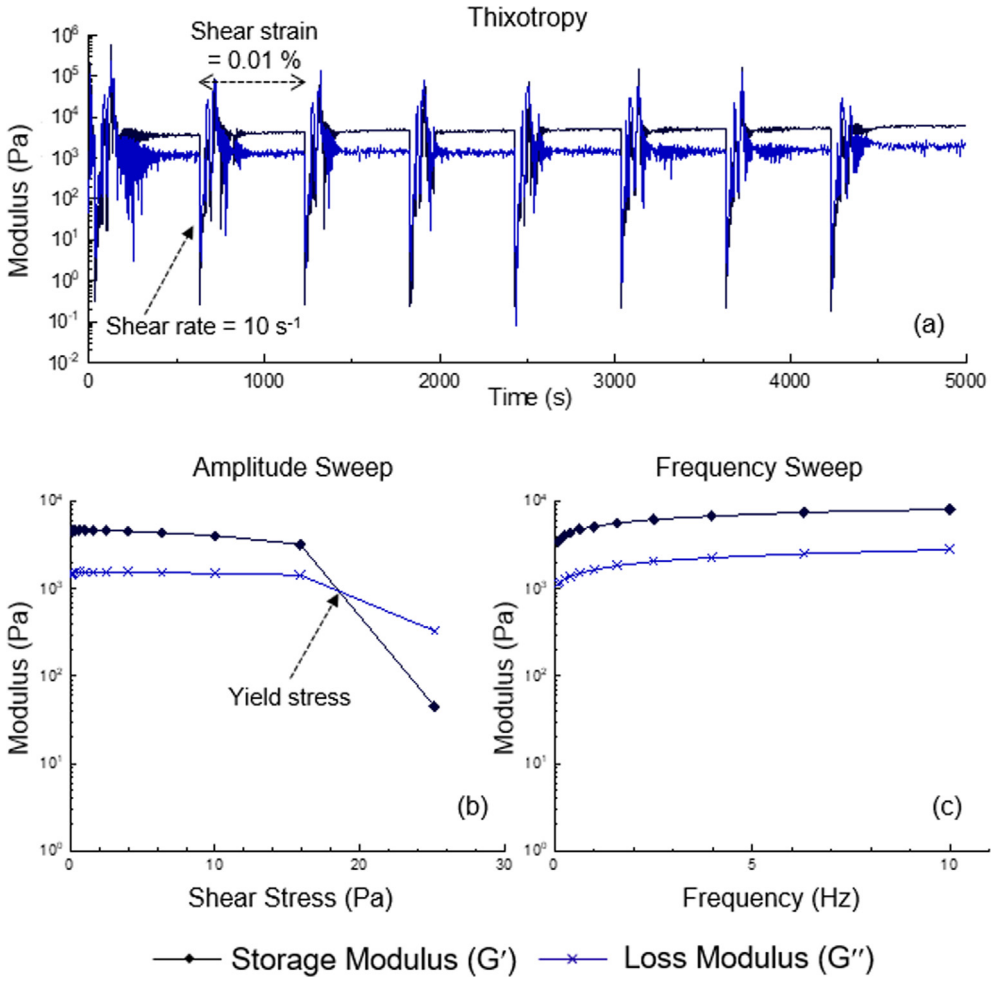

Fig. 5. Oscillatory rheology of the **1·2Cl-HEA** hydrogel (30 mg/ml **1·2Cl**, 2:8 HEA:water, 1.5 mg/ml PI). **(a)** Thixotropy obtained from a cyclic high shear rate-low shear strain rheological process. A total of 8 cycles were applied to the hydrogel; **(b)** plots of stiffness versus shear stress obtained from amplitude sweep at frequency = 1 Hz; and **(c)** plots of stiffness versus frequency obtained from a frequency sweep at stress = 5 Pa.

rates when extruded through the nozzle, and on exit from the nozzle the shear is instantly removed. This rheological thixotropic testing, therefore, resembles (to a certain degree) the shear changes during an extrusion-based 3D printing process. There was no significant change in G′ and G″ after eight cycles of high shear-low shear rheological process. Therefore, the **1·2Cl-HEA** hydrogel showed consistent thixotropic behaviour and rapid recovery under cyclic processing, which is ideal for extrusion-based 3D printing.

The amplitude sweeps of **1·2Cl-HEA** determined a linear viscoelastic region between 0 Pa and about 16 Pa in which the G′ and G″ did not change significantly (Fig. 5(**b**)). The fibre network formed by **1·2Cl** started to break down beyond a yield stress of approximate 18 Pa. Yield stress is where an elastic gel starts converting to a viscous liquid [53]. The yield stress should be a balance between allowing flow of the hydrogel during printing and the stability of the printed structure. The presence of a yield stress could increase the stability of a 3D printed structure. However, if the yield stress is too high, it would cause an excessive pressure drop across the extrusion head. Chemical hydrogels that are covalently bonded often have a yield stress above 100 Pa [62,63]. Physical gels formed from gelator interaction are soft materials on account of the nature of the non-covalent interactions holding them rigid. For example, a previous study investigating the rheology of a similar gelator in a simple solvent system has reported yield stresses of 1.2–8.1 Pa [46]. Therefore, gels formed with **1·2Cl** and similar materials possess lower yield stress compared to covalent bonded hydrogels. The supramolecular network to support multi-layer stacking is ideal for small and medium-sized 3D printed structures, but as we shall see they can provide sufficient strength to allow subsequent formation of a more robust covalent network.

The frequency sweeps of the **1·2Cl-HEA** hydrogel showed G′ > G″ between shear frequencies of 0.4 and 10 Hz (Fig. 5(**c**)). The hydrogels were maintained as elastic gels across the range of shear frequencies. The **1·2Cl-HEA** hydrogel had G′ of 8100 Pa at 10 Hz. Compared to our previous works using similar gelators, this stiffness was greater for this supramolecular material family [43,46]. This relatively high resistance to deformation may be the result of a stiffer network resulting from the combination of supramolecular bonds forming the structure that include the chloride ion and the possibility of its interactions with the novel solvent. Good stiffness prevents significant deformation of the printed structures under layer stacking. Overall, the **1·2Cl-HEA** formulation developed in this study demonstrated excellent rheological behaviour towards extrusion-based 3D printing in every aspect including thixotropy, recovery time, viscoelasticity, yield stress and stiffness.

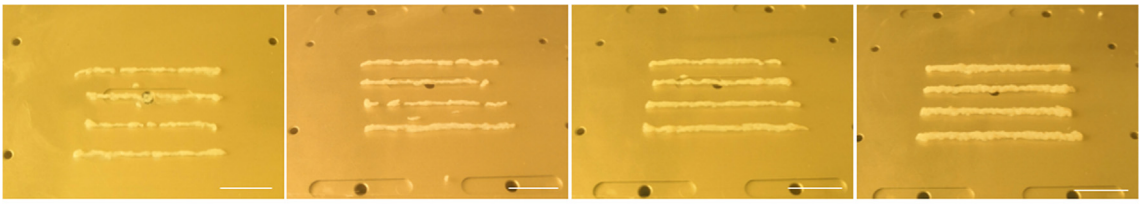

Printing Speed	1st filament	2nd filament	3rd filament	4th filament
5 mm/s	1.07 ± 0.08	1.06 ± 0.05	0.97 ± 0.18	1.10 ± 0.10
7 mm/s	0.78 ± 0.16	0.85 ± 0.06	0.79 ± 0.20	0.97 ± 0.13
10 mm/s	0.66 ± 0.36	0.59 ± 0.29	0.44 ± 0.30	0.85 ± 0.26
15 mm/s	0.42 ± 0.31	0.66 ± 0.29	0.35 ± 0.22	0.55 ± 0.36

Fig. 6. Filament width (mean ± SD) of the **1·2Cl-HEA** hydrogel printed at different speeds from 5 mm/s to 15 mm/s, scale bar = 10 mm.

3.2. 3D printing

Following the development of the **1·2Cl-HEA** formulation, its suitability for extrusion-based 3D printing was investigated. The printhead movement speed was calibrated to correlate with the compressed air pressure applied within the cartridge to ensure a precise control of deposition of the **1·2Cl-HEA** formulation. At printing speeds of 10 and 15 mm/s, an incomplete filament was deposited on the substrate, indicating insufficient deposition (Fig. 6). In general, increasing pressure or reducing printing speed can both address insufficient deposition. However, in the specific case of this **1·2Cl**-containing formulations, increasing pressure was not an ideal approach as it would cause further disassembly of the supramolecular network. Consequently, after deposition the recovery of the gel structure would be delayed as it would take a longer time to re-assemble the fibrillar network. Insufficient deposition did not occur at printing speeds of 5 and 7 mm/s, and the filament width is higher and more consistent with the slower printing speed. A consistent filament width indicated that deposition speed had coincided with the head movement speed. At 5 mm/s printing speed, the height of the filament (0.8 mm) is lower than the width (approximate 1 mm) because of the spreading of the gel. Nevertheless, the layer thickness and printing speed have been determined for processing the **1·2Cl-HEA** formulation. While the printing resolution could be increased by using a printhead with smaller diameter (<0.6 mm), that would require re-investigation of the pressure and printing speed as greater pressure drop will occur as a consequence of using a narrower printhead. Here we focus on the 3D printing process with the 0.6 mm printhead.

Under air, a 60-minute UV curing time was required to achieve >99% reduction in vinyl group of the hydrogel (Fig. 7). As a result, the structure had sufficient strength and stiffness to be handled, e.g. with tweezers (Fig. 7 (**b**)). Free-radical polymerisation of HEA is inhibited by the presence of oxygen as the growing chain will react with molecular oxygen to produce fewer reactive radicals. Curing under an N_2 atmosphere (oxygen level < 1%) gave 100% polymerisation within 20 min. However, this still did not meet the processing requirement if layer-by-layer curing was adopted. The slow curing rates were related to the low concentration of

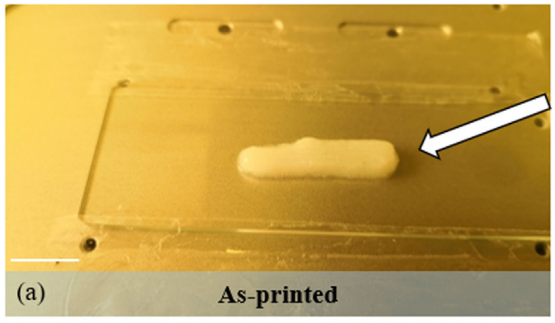

Curing Time (min)	Reduction in Vinyl Group (%)	
	Air	N_2
0	0	0
5	34.12 ± 5.03	64.05 ± 1.43
10	62.55 ± 6.33	72.16 ± 7.82
20	86.74 ± 2.01	100
30	90.10 ± 2.74	100
60	99.16 ± 0.39	100

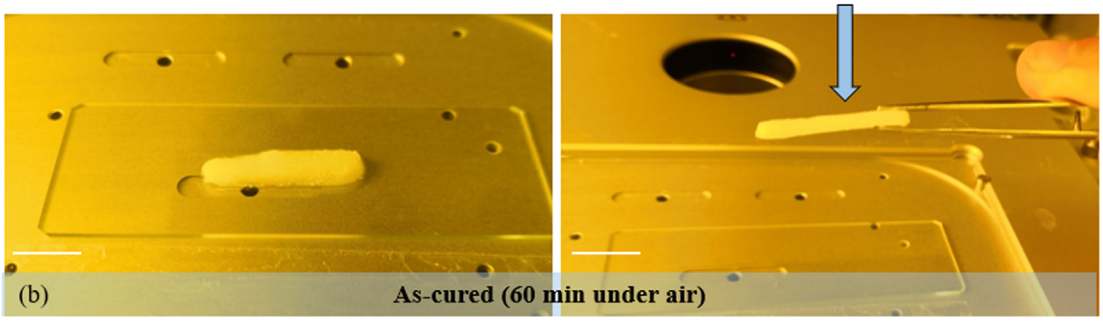

Fig. 7. The reduction in vinyl group (%) of the PHEA in the 3D printed hydrogel after UV exposure for different curing times and under different environment. Scale bar = 10 mm.

monomer that only accounts for 20 vol% in the formulation, as it is common for hydrogels to contain high water content. In general, 3D printing based on UV curing requires the formulation to achieve a high reduction in vinyl groups with a very short curing time so that the deposited materials can rapidly become self-supportive. However, it was not a concern in this study after incorporating the LMWG into the formulation. A self-supportive structure was able to form during the 3D printing process only by the physical crosslinking network from **1·2Cl**. All solvents were entrapped and immobilised within the gelator network without significant leakage. The HEA monomer remained at zero conversion during the process. It was not an issue for the material to have slow curing rates since the whole structure had already been supported. HEA in all layers was cured simultaneously during post-processing. Another significant advantage of this approach is that any 3D printing equipment, even the simplest benchtop model, can be used to process UV-curable hydrogels. A glovebox to create an inert atmosphere is no longer a mandatory requirement. Note that a humid environment is only necessary if the overall processing time is longer than the evaporation rate from the material. A humidifier device similar to that used during the post-processing in this study could also be installed inside the printing chamber to enable large hydrogel structures with high water content during large scale printing processes.

Following the optimisation of processing and post-processing, several different **1·2Cl-PHEA** structures were successfully printed and cured. Here we demonstrate the 3D printability by a multi-layered structure designed to comprise flower-like features that require precise deposition of the gel material (Fig. 8). The details were accurately represented in the structure demonstrating 3D printability. The excellent 3D printing capability from the **1·2Cl-HEA** formulation proves it is a successful approach to using a self-assembled supramolecular network during 3D printing process for subsequent formation of a polymeric network for the whole structure during post-processing.

3.3. Characterisation of the DN hydrogel

The new approach has successfully manufactured a DN hydrogel structure consisting of a non-covalent network (softer component) and a covalent network (harder component). Consequently, it is necessary to investigate the effects of both harder and softer components on the mechanical performances of the **1·2Cl-PHEA** hydrogel. The **1·2Cl-PHEA** had significantly higher tensile properties than PHEA in all properties ($p < 0.05$), including Young's modulus, tensile stress to break, and elongation (Fig. 9(**a**)). The most significant improvement was in the Young's modulus which increased 10-fold from 9.7 ± 0.5 kPa (PHEA) to 99.0 ± 12.1 kPa (**1·2Cl-PHEA**). Tensile stress to break and elongation also increased by 277% and 61%, respectively, by incorporating the LMWG. It has been well documented that DN gels have good mechanical performance even when incorporating a non-covalent network that is generally considered as a soft network [35–40]. Gels comprising only polymeric networks have heterogenous chain lengths resulting in stress concentration on the shortest polymeric chains [36]. It becomes an even more significant issue for hydrogels with high water content, which are basically a solution-like system with a very low density of polymer chains. That is why hydrogels with only one network usually have very weak mechanical properties [36,37]. The DN gels incorporating an LMWG can form highly intertwined networks throughout the material. It reinforces the regions where short polymeric chains are located therefore contributing to the improved homogeneity of the hydrogel [35]. To some extent, these kinds of DN materials resemble natural biological materials such as bones and dentins that also consist of hard and soft components [36]. In this study, a specific DN hydrogel consisting a **1·2Cl** gelator and PHEA has demonstrated improved tensile properties. Note that the addition of gelator network also changed the appearance of PHEA hydrogels from the transparency of an amorphous acrylate polymer to the opaqueness arising from the light scattering of the gelator fibres (Fig. 9(**a**)).

Two curing mechanisms have been compared: (1) conventional layer-by-layer curing during process; and (2) curing all layers simultaneously during post-processing. Better tensile properties were achieved using the new approach proposed in this study (Fig. 9(**b**)). For example, the Young's modulus of hydrogels cured with all layers together was 84.7 ± 12.1 kPa, significantly higher than that of the same hydrogels cured layer-by-layer (34.4 ± 14.0 kPa) ($p < 0.05$). The same trend is seen in tensile stress to break and elongation. The most intrinsic problem of 3D printing is poor coalescence between adjacently deposited layers. Upon deposition, each layer needs to have a rapid solidification via UV curing, cooling, chemical reaction, solvent evaporation and so on. In the case of UV curing, a rapid polymerisation of one layer freezing the move-

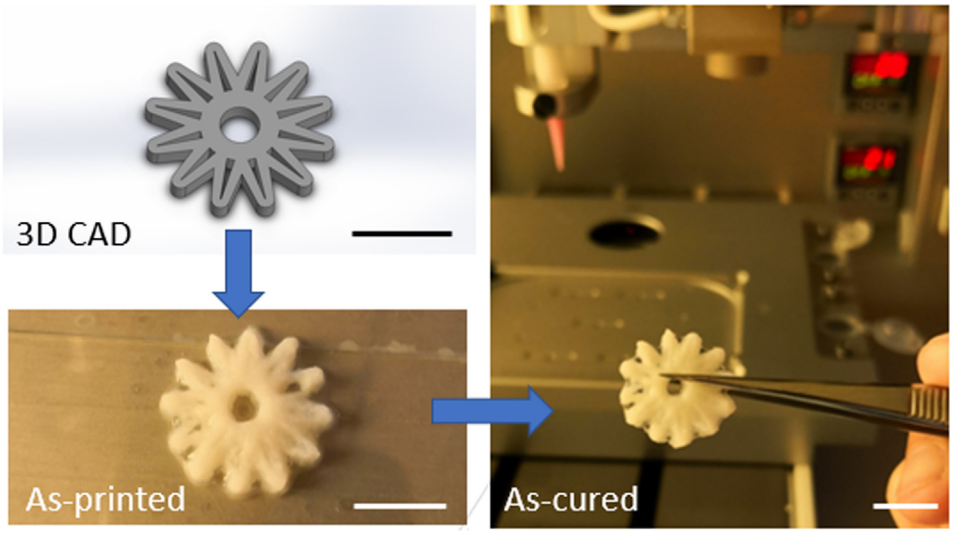

Fig. 8. Demonstration of 3D printability. A flower-shaped structure designed and printed (left) from the **1·2Cl-HEA** formulation and subsequently cured (right) to form **1·2Cl-PHEA**. Scale bar = 10 mm.

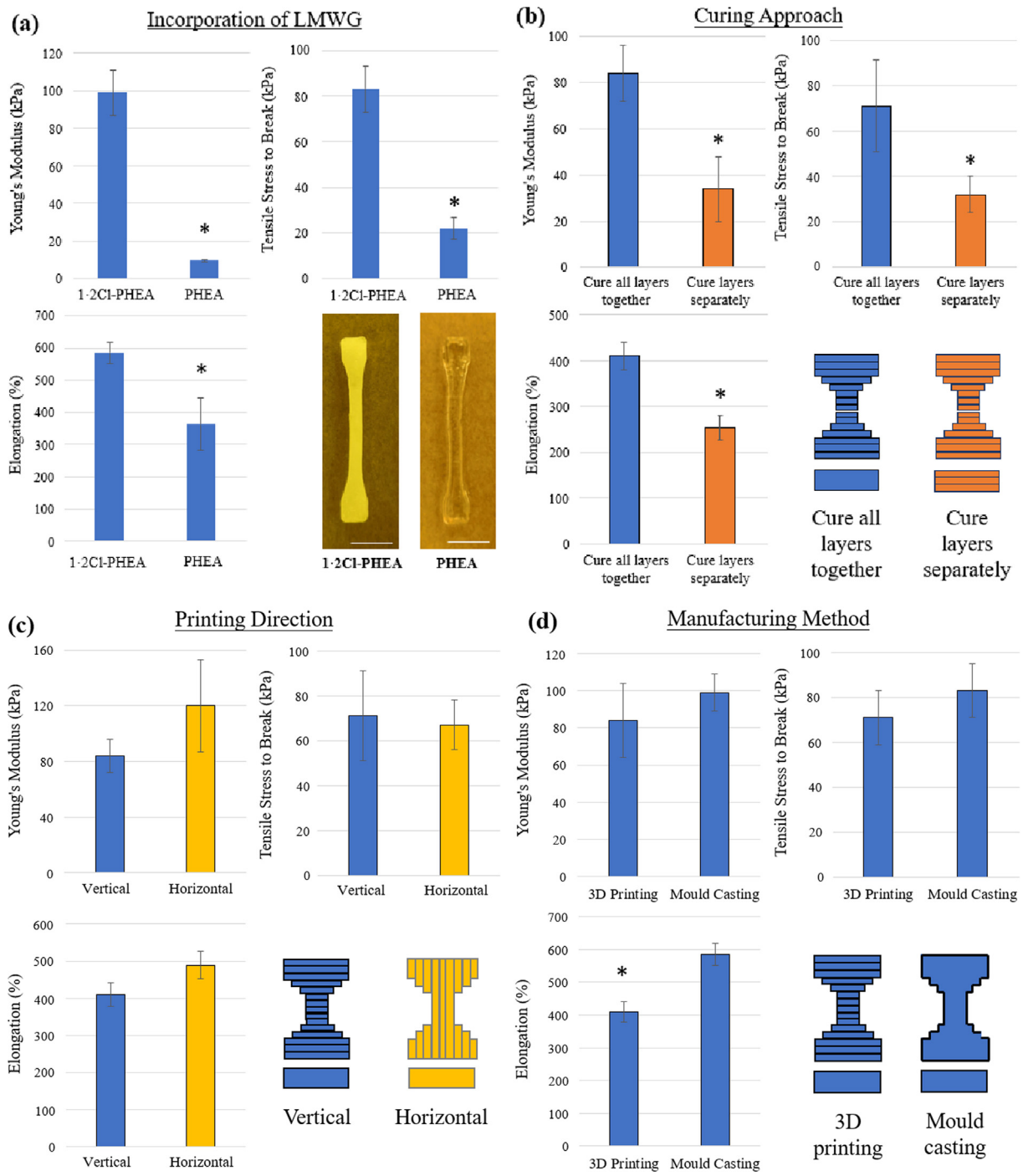

Fig. 9. Tensile properties of (a) **1·2Cl-PHEA** and PHEA hydrogels manufactured using mould casting; (b) 3D printed **1·2Cl-PHEA** hydrogels with different curing approaches; (c) 3D printed **1·2Cl-PHEA** hydrogels with different printing directions; (d) **1·2Cl-PHEA** hydrogels manufactured using 3D printing or mould casting. * denoted to $p < 0.05$ between groups. Scale bar = 5 mm.

ment of polymer chains makes it difficult for the subsequent layer of material to diffuse into the previous layer. Polymer entanglement in the interlayer region is insignificant [23]. Poor interlayer coalescence means that 3D printing is weak in mechanical performance compared to conventional manufacturing methods which form structures as a whole. However, the new approach proposed in this study has made it possible for the whole structure of 3D printed hydrogels to be cured simultaneously. It allows diffusion and arrangement of polymer chains throughout the structure, therefore effectively eliminating the mechanically weak regions between adjacent layers.

Additionally, there was no significant difference in the tensile properties ($p > 0.05$) between hydrogels that had been printed in parallel and perpendicular to the stress direction (Fig. 9(**c**)). This result demonstrates that the materials printed from the **1·2Cl-HEA** formulation are highly homogenous, regardless of the infill pattern. In our approach, the hydrogel structure was only supported by the non-covalent network during the 3D printing pro-

cess. The uniqueness of a non-covalent network is that it is sol–gel reversible. In solution form, gelator molecules diffuse between boundaries of deposited filaments, then the gel forms, rapidly establishing non-covalent interactions to immobilise the solvents. The whole process was repeated every time when a new filament was deposited. Contrarily, polymeric materials extruded using 3D printing can only build heterogeneous structures that are mechanically strong in the printing direction while weak in perpendicular to the printing direction. This characteristic results from the non-reversible bonding of the long-chain molecules that do not have the mobility to diffuse through boundaries as easy as small molecules. Therefore, using the new printing approach proven in this study, homogenously inter-layered and intra-layered structures were fabricated.

The **1·2Cl-PHEA** objects manufactured using 3D printing and mould casting exhibited no significant differences in Young's modulus and tensile stress to break ($p > 0.05$) (Fig. 9(**d**)). The only significant difference was found in elongation between two groups. In general, inadequate mechanical properties of structures fabricated using material extrusion 3D printing techniques are a major challenge that many studies have attempted various approaches to address [64–67]. It is one of the key reasons why material extrusion 3D printing does not compete well with conventional manufacturing in many industrial sectors. This study has successfully improved the mechanical performance of 3D printed hydrogels to the level that is close to conventional manufacturing. It demonstrated highly isotropic structures from the innovative curing strategy benefiting from the **1·2Cl-HEA** formulation.

The co-existence of **1·2Cl** and PHEA networks has been proven by scanning electron microscopy (SEM) and X-ray diffraction (XRD) (Fig. 10). The gelator fibrillar network was visibly embedded in the polymer structure in the SEM image of the objects, confirming the interpenetrating network between **1·2Cl** and PHEA. This morphology was not observed by SEM for a pure PHEA single network. The widths of gelator self-assembled fibres were approximately 150 nm to 400 nm. The physical association and entanglement between the covalent and non-covalent networks are believed to enhance the mechanical properties of the hydrogel, as exhibited in the tensile results. The principal peak of **1·2Cl** fibrillar network in the XRD data was also present in the **1·2Cl-PHEA** diffractogram. Also, in overall, there was no significant shift in the PHEA peaks in the FTIR spectrum of the dual network (Fig. 10(**d**)). These results show that no strong chemical bonds (covalent or non-covalent) were formed between the gelator and polymeric networks that coexist in the material. This finding correlated well with previous studies that demonstrated only physical interaction between gelator and the polymeric network [38,39]. The physical interpenetration of the two networks gives a more robust hydrogel without the downside of modifying chemistry of the functional polymer. This approach is beneficial for many applications requiring specific functionality from 3D printed materials.

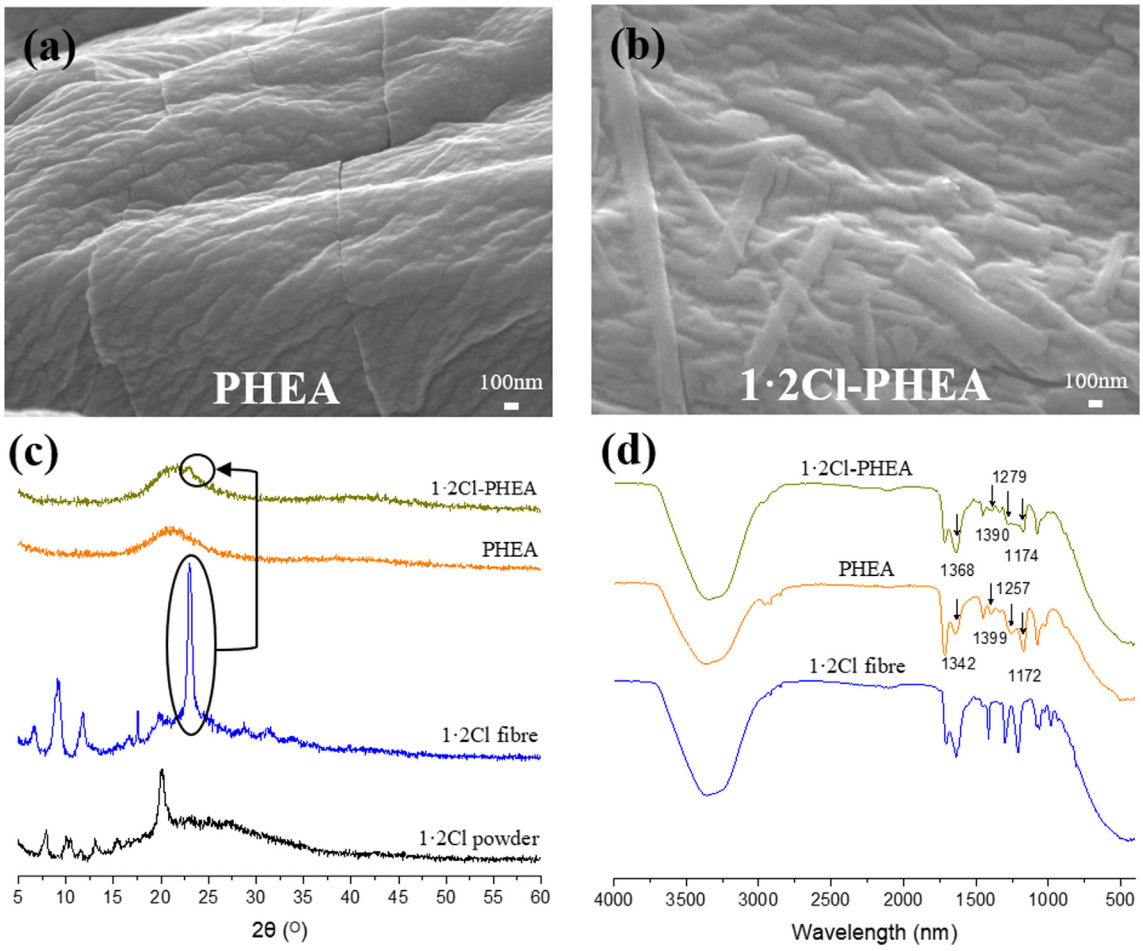

Fig. 10. (**a**-**b**) SEM images of PHEA and **1·2Cl-PHEA** gels, and (**c**) their XRD and (**d**) FTIR spectrum. The peak related to LMWG self-assembled fibrils is highlighted in the XRD data.

In summary, the supramolecular gelator is an excellent material to support 3D printed structures *via* a self-assembled physical network. This property is especially beneficial for UV-curable monomers. Theoretically, a greater variety of monomers can now be 3D printed as long as they can form a thixotropic gel with a specific gelator, of the type shown here or one of the many other family of gelators that are known. The DN hydrogels form interpenetrating networks between softer and harder components and display excellent tensile properties. The DN hydrogel formulation developed in this study provides excellent mechanical properties and increases versatility in material selection for 3D printing process. This achievement is important for the advance in 3D printing products towards better performance and functionalities.

One of the potential applications for the **1·2Cl-PHEA** hydrogels is drug delivery, for example, as a topical treatment of rosacea. A bis-imidazolium-based amphiphile (**1·2Br**) has been used in previous studies to form hydrogels for this specific pharmaceutical application [46,68]. Many drugs including an 4-(2-aminoethyl) benzenesulfonyl fluoride hydrochloride (AEBSF) protease inhibitor have been incorporated in single-network hydrogels for release [46,68]. The potential benefit of using DN hydrogels developed in this study is long-term treatment. 3D printing could be used to fabricate custom face masks that can perfectly fit the face contours of patients. To achieve this goal, a full scale of experiments involving 3D scanning, 3D model development and printing, drug release, skin permeation, drug retention on skin and inside skin, and pharmacological efficacy *in vivo* is foreseen. The current study is a facilitator for applications such as this, showing that (1) the formulation of small molecule gelators with monomers in a solution followed by post-extrusion 3D printing curing gives DN hydrogels, and (2) the interpenetrating interaction between the gelator and polymeric networks in these materials gives rise to isotropic structures not habitually formed by additive manufacturing.

4. Conclusions

In this study, a bis-imidazolium amphiphile gelator **1·2Cl** was mixed with the HEA monomer to form a supramolecular hydrogel that was used for extrusion-based 3D printing. It is a thixotropic gel with rapid recovery, modest yield stress and good stiffness, all ideal for the process. During 3D printing, the overall structure was supported exclusively by the supramolecular network self-assembled *via* inter-gelator interaction. This approach allowed a change in the way photopolymerisation is performed for the 3D printed structures compared with previously known protocols; all layers were cured simultaneously during the postprocessing. Consequently, the inter-layer coalescence significantly improved compared with those printed using a layer-by-layer curing approach. For example, there was more than doubled increase in Young′s modulus (84.7 ± 12.1 kPa to 34.4 ± 14.0 kPa). A better inter-layer coalescence was also achieved thanks to interpenetration of gelator molecules to form supramolecular interactions. Highly isotropic structures were fabricated using this innovative approach. The 3D printed hydrogels have reached the same level of Young′s modulus and stress to break as mould cast samples. The physical association and entanglement between the covalent and non-covalent networks also enhanced the tensile properties of the hydrogel. Young′s modulus increased 10-fold from 9.7 ± 0. 5 kPa (PHEA) to 99.0 ± 12.1 kPa (**1·2Cl-PHEA**). The innovative approach using a supramolecular network to support a structure can increase the variety in material selection for 3D printing. Different gelator chemistry and triggering mechanisms have a great potential to be used in different 3D printing techniques, such as vat polymerisation, material jetting and material extrusion. The DN hydrogel fabricated using this approach has excellent mechanical performance potentially providing benefit for a range of applications, including for example, those in the medical and healthcare fields.

5. Associated content

Synthesis procedure and chemical characterisation of the **1·2Cl** gelator.

CRediT authorship contribution statement

Zuoxin Zhou: Methodology, Formal analysis, Investigation, Writing - original draft. **Mario Samperi:** Writing - original draft, Methodology. **Lea Santu:** Methodology, Investigation. **Glenieliz Dizon:** Investigation. **Shereen Aboarkaba:** Conceptualization. **David Limón:** Conceptualization, Methodology, Formal analysis. **David Limón:** . **Christopher Tuck:** Conceptualization, Writing - review & editing, Funding acquisition, Supervision. **Lluïsa Pérez-García:** Conceptualization, Writing - review & editing, Funding acquisition. **Derek J. Irvine:** Conceptualization, Funding acquisition, Supervision. **David B. Amabilino:** Conceptualization, Writing - review & editing, Funding acquisition, Supervision. **Ricky Wildman:** Conceptualization, Writing - review & editing, Funding acquisition, Project administration, Supervision.

Declaration of Competing Interest

The authors declare that they have no known competing financial interests or personal relationships that could have appeared to influence the work reported in this paper.

Acknowledgements

The authors acknowledge funding from the EPSRC (Engineering and Physical Sciences Research Council) via research grant EP/N024818/1 titled ‘Formulation for 3D Printing: Creating a Plug and Play Platform for a Disruptive UK Industry’. We thank The Nanoscale and Microscale Research Centre (nmRC) at the University of Nottingham for facilitating the SEM imaging. D.B.A thanks the EPSRC (project EP/M005178/1) and the School of Chemistry at the University of Nottingham for funding. D.L. and L.P.G thank the EU ERDF (FEDER) funds and the Spanish Government grant TEC2017-85059-C3-2-R. We thank Prof. Morgan Alexander, Prof. Clive Roberts, and Prof. Richard Hague from the University of Nottingham for their constructive advice on the project and manuscript.

Appendix A. Supplementary material

Supplementary data to this article can be found online at https://doi.org/10.1016/j.matdes.2021.109792.

References

[1] F.P. Melchels, J. Feijen, D.W. Grijpma, A review on stereolithography and its applications in biomedical engineering, Biomaterials 31 (24) (2010) 6121–6130.
[2] J.R. Tumbleston, D. Shirvanyants, N. Ermoshkin, R. Janusziewicz, A.R. Johnson, D. Kelly, K. Chen, R. Pinschmidt, J.P. Rolland, A. Ermoshkin, Continuous liquid interface production of 3D objects, Science 347 (6228) (2015) 1349–1352.
[3] Z. Zhou, L.R. Cantu, X. Chen, M.R. Alexander, C.J. Roberts, R. Hague, C. Tuck, D. Irvine, R. Wildman, High-throughput characterization of fluid properties to predict droplet ejection for three-dimensional inkjet printing formulations, Addit. Manuf. 29 (2019) 100792.
[4] F. Yang, V. Tadepalli, B.J. Wiley, 3D printing of a double network hydrogel with a compression strength and elastic modulus greater than those of cartilage, ACS Biomater. Sci. Eng. 3 (5) (2017) 863–869.

[5] Y. Liu, Q. Hu, F. Zhang, C. Tuck, D. Irvine, R. Hague, Y. He, M. Simonelli, G.A. Rance, E.F. Smith, Additive manufacture of three dimensional nanocomposite based objects through multiphoton fabrication, Polymers 8 (9) (2016) 325.
[6] C.E. Hoyle, Photocurable Coatings, ACS Publications, 1990.
[7] M. Zarek, M. Layani, I. Cooperstein, E. Sachyani, D. Cohn, S. Magdassi, 3D printing of shape memory polymers for flexible electronic devices, Adv. Mater. 28 (22) (2016) 4449–4454.
[8] A.A. Pawar, G. Saada, I. Cooperstein, L. Larush, J.A. Jackman, S.R. Tabaei, N.-J. Cho, S. Magdassi, High-performance 3D printing of hydrogels by water-dispersible photoinitiator nanoparticles, Sci. Adv. 2 (4) (2016) e1501381.
[9] D.M. Kirchmajer, R. Gorkin Iii, An overview of the suitability of hydrogel-forming polymers for extrusion-based 3D-printing, J. Mater. Chem. B 3 (20) (2015) 4105–4117.
[10] T.M. Lovestead, A.K. O'Brien, C.N. Bowman, Models of multivinyl free radical photopolymerization kinetics, J. Photochem. Photobiol., A 159 (2) (2003) 135–143.
[11] A. Bagheri, J. Jin, Photopolymerization in 3D printing, ACS Appl. Polym. Mater. 1 (4) (2019) 593–611.
[12] M. Layani, X. Wang, S. Magdassi, Novel materials for 3D printing by photopolymerization, Adv. Mater. 30 (41) (2018) 1706344.
[13] H. Quan, T. Zhang, H. Xu, S. Luo, J. Nie, X. Zhu, Photo-curing 3D printing technique and its challenges, Bioact. Mater. 5 (1) (2020) 110–115.
[14] I.V. Khudyakov, J.C. Legg, M.B. Purvis, B.J. Overton, Kinetics of Photopolymerization of Acrylates with Functionality of 1–6, Ind. Eng. Chem. Res. 38 (9) (1999) 3353–3359.
[15] M.J. Troughton, Handbook of Plastics Joining: A Practical Guide, William Andrew, 2008.
[16] J.-W. Park, J.-G. Lee, G.-S. Shim, H.-J. Kim, Y.-K. Kim, S.-E. Moon, D.-H. No, Evaluation of the ultraviolet-curing kinetics of ultraviolet-polymerized oligomers cured using poly (ethylene glycol) dimethacrylate, Coatings 8 (3) (2018) 99.
[17] C. Credi, A. Fiorese, M. Tironi, R. Bernasconi, L. Magagnin, M. Levi, S. Turri, 3D printing of cantilever-type microstructures by stereolithography of ferromagnetic photopolymers, ACS Appl. Mater. Interfaces 8 (39) (2016) 26332–26342.
[18] J. Warner, P. Soman, W. Zhu, M. Tom, S. Chen, Design and 3D printing of hydrogel scaffolds with fractal geometries, ACS Biomater. Sci. Eng. 2 (10) (2016) 1763–1770.
[19] R. Liska, M. Schuster, R. InfŘhr, C. Turecek, C. Fritscher, B. Seidl, V. Schmidt, L. Kuna, A. Haase, F. Varga, Photopolymers for rapid prototyping, J. Coat. Technol. Res. 4 (4) (2007) 505–510.
[20] A. Tofangchi, P. Han, J. Izquierdo, A. Iyengar, K. Hsu, Effect of Ultrasonic Vibration on Interlayer Adhesion in Fused Filament Fabrication 3D Printed ABS, Polymers 11 (2) (2019) 315.
[21] H. Kim, S. Han, Y. Seo, Novel Dual-Curing Process for a Stereolithographically Printed Part Triggers a Remarkably Improved Interlayer Adhesion and Excellent Mechanical Properties, Langmuir 36 (31) (2020) 9250–9258.
[22] A.M. Pekkanen, R.J. Mondschein, C.B. Williams, T.E. Long, 3D printing polymers with supramolecular functionality for biological applications, Biomacromolecules 18 (9) (2017) 2669–2687.
[23] Z. Zhou, I. Salaoru, P. Morris, G.J. Gibbons, Additive manufacturing of heat-sensitive polymer melt using a pellet-fed material extrusion, Addit. Manuf. 24 (2018) 552–559.
[24] S.H. Ahn, M. Montero, D. Odell, S. Roundy, P.K. Wright, Anisotropic material properties of fused deposition modeling ABS, Rapid Prototyping J. (2002).
[25] O. Es-Said, J. Foyos, R. Noorani, M. Mendelson, R. Marloth, B. Pregger, Effect of layer orientation on mechanical properties of rapid prototyped samples, Mater. Manuf. Processes 15 (1) (2000) 107–122.
[26] C.B. Highley, C.B. Rodell, J.A. Burdick, Direct 3D printing of shear-thinning hydrogels into self-healing hydrogels, Adv. Mater. 27 (34) (2015) 5075–5079.
[27] N.P. Levenhagen, M.D. Dadmun, Improving Interlayer Adhesion in 3D Printing with Surface Segregating Additives: Improving the Isotropy of Acrylonitrile–Butadiene–Styrene Parts, ACS Appl. Polym. Mater. 1 (4) (2019) 876–884.
[28] N.P. Levenhagen, M.D. Dadmun, Interlayer diffusion of surface segregating additives to improve the isotropy of fused deposition modeling products, Polymer 152 (2018) 35–41.
[29] L. Ouyang, J.P. Armstrong, Y. Lin, J.P. Wojciechowski, C. Lee-Reeves, D. Hachim, K. Zhou, J.A. Burdick, M.M. Stevens, Expanding and optimizing 3D bioprinting capabilities using complementary network bioinks, Sci. Adv. 6 (38) (2020) eabc5529.
[30] D.J. Cornwell, B.O. Okesola, D.K. Smith, Hybrid polymer and low molecular weight gels–dynamic two-component soft materials with both responsive and robust nanoscale networks, Soft Matter 9 (36) (2013) 8730–8736.
[31] D.J. Cornwell, D.K. Smith, Expanding the scope of gels–combining polymers with low-molecular-weight gelators to yield modified self-assembling smart materials with high-tech applications, Mater. Horiz. 2 (3) (2015) 279–293.
[32] D.B. Amabilino, D.K. Smith, J.W. Steed, Supramolecular materials, Chem. Soc. Rev. 46 (9) (2017) 2404–2420.
[33] A. Chalard, M. Mauduit, S. Souleille, P. Joseph, L. Malaquin, J. Fitremann, 3D printing of a biocompatible low molecular weight supramolecular hydrogel by dimethylsulfoxide water solvent exchange, Addit. Manuf. (2020) 101162.
[34] M.C. Nolan, A.M.F. Caparrós, B. Dietrich, M. Barrow, E.R. Cross, M. Bleuel, S.M. King, D.J. Adams, Optimising low molecular weight hydrogels for automated 3D printing, Soft Matter 13 (45) (2017) 8426–8432.
[35] L. Tang, D. Zhang, L. Gong, Y. Zhang, S. Xie, B. Ren, Y. Liu, F. Yang, G. Zhou, Y. Chang, Double-Network Physical Cross-Linking Strategy To Promote Bulk Mechanical and Surface Adhesive Properties of Hydrogels, Macromolecules 52 (24) (2019) 9512–9525.
[36] Q. Chen, H. Chen, L. Zhu, J. Zheng, Fundamentals of double network hydrogels, J. Mater. Chem. B 3 (18) (2015) 3654–3676.
[37] J.P. Gong, Why are double network hydrogels so tough?, Soft Matter 6 (12) (2010) 2583–2590.
[38] F. Chen, Z. Tang, S. Lu, L. Zhu, Q. Wang, Q. Gang, J. Yang, Q. Chen, Fabrication and mechanical behaviors of novel supramolecular/polymer hybrid double network hydrogels, Polymer 168 (2019) 159–167.
[39] F. Chen, Q. Chen, L. Zhu, Z. Tang, Q. Li, G. Qin, J. Yang, Y. Zhang, B. Ren, J. Zheng, General strategy to fabricate strong and tough low-molecular-weight gelator-based supramolecular hydrogels with double network structure, Chem. Mater. 30 (5) (2018) 1743–1754.
[40] J. Hao, Y. Gao, J. Liu, J. Hu, Y. Ju, S. Tough, Compressive Double Network Hydrogel Using Natural Glycyrrhizic Acid Tailored Low-Molecular-Weight Gelator Strategy. In Situ Spontaneous Formation of Au Nanoparticles To Generate a Continuous Flow Reactor, ACS Appl. Mater. Interfaces 12 (4) (2019) 4927–4933.
[41] Q. Wang, J.L. Mynar, M. Yoshida, E. Lee, M. Lee, K. Okuro, K. Kinbara, T. Aida, High-water-content mouldable hydrogels by mixing clay and a dendritic molecular binder, Nature 463 (7279) (2010) 339–343.
[42] M. Rodrigues, A.C. Calpena, D.B. Amabilino, M.L. Garduño-Ramírez, L. Pérez-García, Supramolecular gels based on a gemini imidazolium amphiphile as molecular material for drug delivery, J. Mater. Chem. B 2 (33) (2014) 5419–5429.
[43] M. Samperi, D. Limón, D.B. Amabilino, L. Pérez-García, Enhancing Singlet Oxygen Generation by Self-Assembly of a Porphyrin Entrapped in Supramolecular Fibers, Cell Rep. Phys. Sci. (2020) 100030.
[44] M. Samperi, L. Pérez-García, D.B. Amabilino, Quantification of energy of activation to supramolecular nanofibre formation reveals enthalpic and entropic effects and morphological consequence, Chem. Sci. 10 (44) (2019) 10256–10266.
[45] S. Giraldo, M.E. Alea-Reyes, D. Limón, A. González, M. Duch, J.A. Plaza, D. Ramos-López, J. de Lapuente, A. González-Campo, L. Pérez-García, π-Donor/π-Acceptor Interactions for the Encapsulation of Neurotransmitters on Functionalized Polysilicon-Based Microparticles, Pharmaceutics 12 (8) (2020) 724.
[46] D. Limón, C. Jiménez-Newman, M. Rodrigues, A. González-Campo, D.B. Amabilino, A.C. Calpena, L. Pérez-García, Cationic supramolecular hydrogels for overcoming the skin barrier in drug delivery, ChemistryOpen 6 (4) (2017) 585.
[47] H. Jiang, L. Duan, X. Ren, G. Gao, Hydrophobic association hydrogels with excellent mechanical and self-healing properties, Eur. Polym. J. 112 (2019) 660–669.
[48] J. Chen, R. An, L. Han, X. Wang, Y. Zhang, L. Shi, R. Ran, Tough hydrophobic association hydrogels with self-healing and reforming capabilities achieved by polymeric core-shell nanoparticles, Mater. Sci. Eng., C 99 (2019) 460–467.
[49] S. Bhattacharya, U. Maitra, S. Mukhopadhyay, A. Srivastava, Advances in molecular hydrogels, in: Molecular Gels, Springer, 2006, pp. 613–647.
[50] T. Speck, G. Bauer, F. Flues, K. Oelker, M. Rampf, A.C. Schüssele, M. von Tapavicza, J. Bertling, R. Luchsinger, A. Nellesen, Bio-inspired self-healing materials, Mater. Design Inspired by Nature (2013) 359–389.
[51] H. Li, Y.J. Tan, K.F. Leong, L. Li, 3D bioprinting of highly thixotropic alginate/methylcellulose hydrogel with strong interface bonding, ACS Appl. Mater. Interfaces 9 (23) (2017) 20086–20097.
[52] H. Li, S. Liu, L. Lin, Rheological study on 3D printability of alginate hydrogel and effect of graphene oxide, Int. J. Bioprinting 2 (2) (2016).
[53] J.M. Townsend, E.C. Beck, S.H. Gehrke, C.J. Berkland, M.S. Detamore, Flow behavior prior to crosslinking: The need for precursor rheology for placement of hydrogels in medical applications and for 3D bioprinting, Prog. Polym. Sci. 91 (2019) 126–140.
[54] F. Sánchez-Correa, C. Vidaurre-Agut, Á. Serrano-Aroca, A.J. Campillo-Fernández, Poly (2-hydroxyethyl acrylate) hydrogels reinforced with graphene oxide: Remarkable improvement of water diffusion and mechanical properties, J. Appl. Polym. Sci. 135 (15) (2018) 46158.
[55] M. Lin, P. Xu, W. Zhong, Preparation, characterization, and release behavior of aspirin-loaded poly (2-hydroxyethyl acrylate)/silica hydrogels, J. Biomed. Mater. Res. B Appl. Biomater. 100 (4) (2012) 1114–1120.
[56] M.M. Pradas, J.G. Ribelles, A.S. Aroca, G.G. Ferrer, J.S. Antón, P. Pissis, Interaction between water and polymer chains in poly (hydroxyethyl acrylate) hydrogels, Colloid Polym. Sci. 279 (4) (2001) 323–330.
[57] J.S. Vuković, A.A. Perić-Grujić, D.S. Mitić-Ćulafić, B.D.B. Nedeljković, S.L. Tomić, Antibacterial activity of pH-sensitive silver (I)/poly (2-hydroxyethyl acrylate/itaconic acid) hydrogels, Macromol. Res. 28 (4) (2020) 382–389.
[58] R.K. Mishra, A.R. Ray, Synthesis and characterization of poly N-[3-(dimethylamino) propyl] methacrylamide-co-itaconic acid hydrogels for drug delivery, J. Appl. Polym. Sci. 119 (6) (2011) 3199–3206.
[59] T. Çaykara, M. Demiray, O. Güven, Effect of type and concentration of surfactants on swelling behavior of poly [N-[3-(dimethylamino) propyl] methacrylamide-co-N, N-methylenebis (acrylamide)] hydrogels, Colloid Polym. Sci. 284 (3) (2005) 258–265.
[60] M. Andac, F. Plieva, A. Denizli, I.Y. Galaev, B. Mattiasson, Poly (hydroxyethyl methacrylate)-based macroporous hydrogels with disulfide cross-linker, Macromol. Chem. Phys. 209 (6) (2008) 577–584.
[61] D. Noferini, A. Faraone, M. Rossi, E. Mamontov, E. Fratini, P. Baglioni, Disentangling polymer network and hydration water dynamics in

polyhydroxyethyl methacrylate physical and chemical hydrogels, J. Phys. Chem. C 123 (31) (2019) 19183–19194.
[62] E.C. Beck, M. Barragan, M.H. Tadros, E.A. Kiyotake, F.M. Acosta, S.L. Kieweg, M. S. Detamore, Chondroinductive hydrogel pastes composed of naturally derived devitalized cartilage, Ann. Biomed. Eng. 44 (6) (2016) 1863–1880.
[63] A.K. Gaharwar, R.K. Avery, A. Assmann, A. Paul, G.H. McKinley, A. Khademhosseini, B.D. Olsen, Shear-thinning nanocomposite hydrogels for the treatment of hemorrhage, ACS Nano 8 (10) (2014) 9833–9842.
[64] T. Rahim, A. Abdullah, H.M. Akil, D. Mohamad, Z. Rajion, The improvement of mechanical and thermal properties of polyamide 12 3D printed parts by fused deposition modelling, eXPRESS Polym. Lett. 11 (12) (2017) 963–982.
[65] A.C. Uzcategui, A. Muralidharan, V.L. Ferguson, S.J. Bryant, R.R. McLeod, Understanding and improving mechanical properties in 3D printed parts using a dual-cure acrylate-based resin for stereolithography, Adv. Eng. Mater. 20 (12) (2018) 1800876.
[66] Z. Zhou, E. Cunningham, A. Lennon, H.O. McCarthy, F. Buchanan, S.A. Clarke, N. Dunne, Effects of poly (ε-caprolactone) coating on the properties of three-dimensional printed porous structures, J. Mech. Behav. Biomed. Mater. 70 (2017) 68–83.
[67] Z. Zhou, A. Lennon, F. Buchanan, H.O. McCarthy, N. Dunne, Binder jetting additive manufacturing of hydroxyapatite powders: Effects of adhesives on geometrical accuracy and green compressive strength, Addit. Manuf. (2020) 101645.
[68] D. Limón, C. Jiménez-Newman, A.C. Calpena, A. González-Campo, D.B. Amabilino, L. Pérez-García, Microscale coiling in bis-imidazolium supramolecular hydrogel fibres induced by the release of a cationic serine protease inhibitor, Chemical Communications 53 (32) (2017) 4509–4512. Submitted for publication.